



Plane strain pure bending of sheets with damage evolution at large strains

Sergei Alexandrov^{a,*}, Jean-Claude Gelin^b

^a A.Yu. Ishlinskii Institute for Problems in Mechanics, Russian Academy of Sciences, 101-1 Prospect Vernadskogo, 119526 Moscow, Russia

^b University of Franche-Comte, FEMTO-ST Institute: Applied Mechanics Department, 24 Rue de l'Épitaphe, 25000 Besançon, France

ARTICLE INFO

Article history:

Received 27 October 2010

Received in revised form 7 February 2011

Available online 15 February 2011

Keywords:

Pure bending

Large strains

Rigid plasticity

Damage evolution

ABSTRACT

An analysis of plane-strain bending at large strains for the rigid/plastic incompressible material model including arbitrary strain-hardening and damage evolution laws is performed. The fracture criterion is based on a critical value of the damage parameter. Numerical treatment is reduced to the system of two partial differential equations written in characteristic coordinates. The through-thickness distribution of the principal stresses and damage parameter as well as the variation of the bending moment with the radius of curvature of the concave surface are found for Swift's hardening law and one specific damage evolution law. General tendencies in solution behaviour are in agreement with physical expectations.

© 2011 Elsevier Ltd. All rights reserved.

1. Introduction

Pure plane-strain bending at large strains is one of the classical problems in plasticity theory. A number of analytical and semi-analytical solutions have been proposed for various rigid- and elastic–plastic models in the literature (Dadras and Majless, 1982; Gao, 1994; Hill, 1950; Lyamina, 2006; Tan et al., 1995; Verguts and Sowerby, 1975; Wang et al., 1993). Individual approaches for solving the boundary value problem dependent of the material model adopted have been developed in these papers. In contrast to these approaches, a unified method for isotropic materials has been proposed in Alexandrov et al. (2006). The only requirement imposed on the system of constitutive equations is that the material is incompressible. The method has been extended to a class of anisotropic materials in Alexandrov and Hwang (2009) and has been successfully used for springback calculation in the case of elastic–plastic non-linear hardening materials in Alexandrov and Hwang (2010). In particular, it has been shown in Alexandrov and Hwang (2009, 2010) that an effect of elasticity at large strains is negligible, even though the distribution of stress is discontinuous in rigid plastic solutions, unless the stage of unloading is of interest. Therefore, a rigid plastic model is adopted in the present paper. A great number of material models have been proposed to account for damage evolution at large strains. One of most important areas of application of such models is ductile fracture prediction in metal forming processes. These models can be divided into three groups. The first group includes uncoupled models in the sense that the damage evolution equation should be solved after the solution to the boundary value problem of plasticity theory is

found. A review of models of this group is given in Atkins (1996). Models of the second group are partly coupled in the sense that the damage parameter reduces the yield surface but material is plastically incompressible. The present paper deals with this group of models and a short review of such models is provided below. Finally, models of the third group are fully coupled in the sense that the damage parameter enters all the constitutive equations of the original model of plasticity theory. In particular, the equation of incompressibility is not satisfied in this case. A typical model of this group has been proposed by Gurson (1977) and then modified by Tvergaard and Needleman (1984) among others. Even though models of the third group are most sophisticated, models of the second group result in better predictions for some applications (Hambli, 2001). Also, models of the second group provide reliable predictions of ductile fracture in metal forming (Behrens and Just, 2002). Therefore, the second group of models is considered in the present paper. Since the equation of incompressibility is valid for such models, the approach developed in Alexandrov et al. (2006) can be adopted to study the pure bending process. The main difference between various damage evolution models of the second group is the damage evolution equation. The most widely used damage evolution equation has been proposed by Lemaitre (1985). The original version of this model includes elastic compressibility but its rigid plastic version is also used in application to metal forming processes (Andrade Pires et al., 2003). Other damage evolution equations coupled with rigid plastic models have been proposed, for example, in Bonora (1997), Chandrakanth and Pandey (1993), Hartley et al. (1997), and Tai (1990). The present paper deals with an extension of the approach to analysis of plane-strain pure bending proposed in Alexandrov et al. (2006) to include quite an arbitrary damage evolution equation in the case of rigid-plastic incompressible materials. An advantage of this ap-

* Corresponding author. Tel.: +7 495 4343665; fax: +7 499 7399531.

E-mail address: sergei_alexandrov@yahoo.com (S. Alexandrov).

proach is that the original boundary value problem is reduced to a simple system of two partial hyperbolic differential equations written in characteristic coordinates. The key point of this successful transformation is a simple mapping between Lagrangian and Eulerian coordinate systems found in Alexandrov et al. (2006). The general analytic derivation and the numerical code developed are valid for any model of the class considered. Specific illustrative calculation is carried out for the damage evolution equation given in Hartley et al. (1997).

Even though strains in the pure bending process are in general rather small, a special technique has been developed in Boers et al. (2010) that allows for large strains in this process. Therefore, the theoretical solution given in the present paper can be combined with this technique to result in a theoretical/experimental method for determining material properties.

2. Kinematics

The approach proposed in Alexandrov et al. (2006) is based on the mapping between Eulerian Cartesian coordinates (x, y) and Lagrangian coordinates (ζ, η) in the form

$$\frac{x}{H} = \sqrt{\frac{\zeta}{a} + \frac{s}{a^2}} \cos(2a\eta) - \frac{\sqrt{s}}{a} \quad \text{and} \quad \frac{y}{H} = \sqrt{\frac{\zeta}{a} + \frac{s}{a^2}} \sin(2a\eta), \quad (1)$$

where H is the initial thickness of the sheet, s is an arbitrary function of a , a is a function of the time, t , and $a = 0$ at $t = 0$. At the initial instant, $a = 0$,

$$s = 1/4. \quad (2)$$

Substituting Eq. (2) into Eq. (1) and applying l'Hospital's rule gives $x = \zeta H$ and $y = \eta H$ at the initial instant when the shape of the specimen is the rectangle defined by the equations $x = -H$, $x = 0$ and $y = \pm L$. The initial shape and the Cartesian coordinate system are shown in Fig. 1. It is possible to assume, with no loss of generality, that the origin of this coordinate system is located at the intersection of the axis of symmetry and surface AB throughout the process of deformation. An intermediate shape is also shown in Fig. 1. It is obvious that $\zeta = 0$ for AB and $\zeta = -1$ for CD throughout the process of deformation. According to Eq. (1), any intermediate shape is determined by two circular arcs, AB and CD , and two straight lines, AD and CB . These circular arcs coincide with coordinate curves of the plane polar coordinate system $r\theta$ defined by the following transformation equations

$$\frac{r}{H} = \sqrt{\frac{\zeta}{a} + \frac{s}{a^2}} \quad \text{and} \quad \theta = 2a\eta. \quad (3)$$

Geometric parameters of the shape at any instant are given by (Fig. 1)

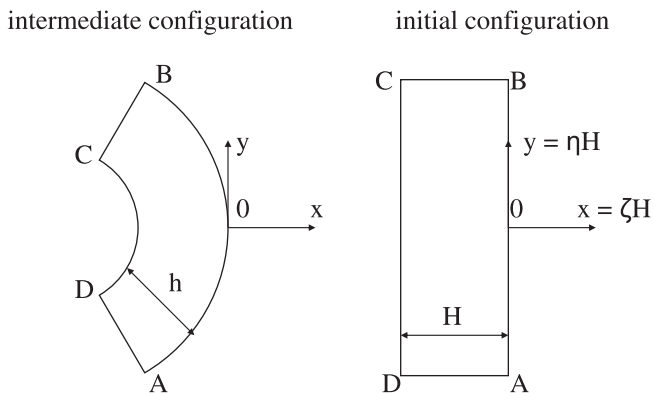


Fig. 1. Coordinate systems, initial shape and intermediate shape in pure bending.

$$\frac{R_{AB}}{H} = \frac{\sqrt{s}}{a}, \quad \frac{R_{CD}}{H} = \sqrt{\frac{s}{a^2} - \frac{1}{a}}, \quad \frac{h}{H} = \frac{\sqrt{s} - \sqrt{s-a}}{a}, \quad (4)$$

where R_{AB} is the radius of surface AB , R_{CD} is the radius of surface CD , and h is the current thickness.

It is possible to verify by inspection that the Lagrangian coordinates coincide with trajectories of the principal strain rates and that the mapping (1) satisfies the equation of incompressibility at any instant. It will be shown in the next section that the assumption that the Lagrangian coordinates coincide with the trajectories of the stress tensor allows one to solve the stress equations. In the case under consideration these two conditions (coincidence of the trajectories for the principal stress and principal strain rate tensors and the equation of incompressibility) are equivalent to the associated flow rule of the classical rate formulation of plasticity theory.

The strain rate components can be found from Eq. (1) and, then, the position of the neutral line is determined by

$$\zeta = \zeta_n = -\frac{ds}{da}, \quad (5)$$

the equivalent strain rate by

$$\dot{\epsilon}_{eq} = \frac{|\zeta + ds/da|}{\sqrt{3}(\zeta a + s)} \frac{da}{dt} \quad (6)$$

and the equivalent strain by

$$\begin{aligned} \epsilon_{eq} &= \frac{1}{\sqrt{3}} \ln[4(\zeta a + s)], \\ \epsilon_{eq} &= \frac{1}{\sqrt{3}} \ln \left\{ \frac{\zeta a + s}{4[\zeta a_c(\zeta) + s_c(\zeta)]^2} \right\}, \\ \epsilon_{eq} &= -\frac{1}{\sqrt{3}} \ln[4(\zeta a + s)] \end{aligned} \quad (7)$$

in regions 1, 2 and 3, respectively. In region 1, $0 \geq \zeta \geq -1/2$, the principal strain rate $\dot{\epsilon}_{\zeta\zeta} < 0$ (and $\dot{\epsilon}_{\eta\eta} > 0$) during the entire process. In region 3, $-1 \leq \zeta \leq \zeta_n^f$, the principal strain rate $\dot{\epsilon}_{\zeta\zeta} > 0$ (and $\dot{\epsilon}_{\eta\eta} < 0$) during the entire process. A property of all curves $\zeta = \text{const}$ in region 2, $\zeta_n^f \leq \zeta \leq -1/2$, is that each of these curves coincides with the neutral line at one time instant. Consider any ζ -curve of this class and denote a_c the value of a at which the curve coincides with the neutral line. Then, $\dot{\epsilon}_{\zeta\zeta} < 0$ ($\dot{\epsilon}_{\eta\eta} > 0$) at $a < a_c$ and $\dot{\epsilon}_{\zeta\zeta} > 0$ ($\dot{\epsilon}_{\eta\eta} < 0$) at $a > a_c$ for this curve. Obviously, the time instant at which the sign is changed depends on the curve such that $a_c = a_c(\zeta)$. The corresponding value of s will be denoted by $s_c(\zeta)$ where $s_c(\zeta) = s[a_c(\zeta)]$. These values of $a_c(\zeta)$ and $s_c(\zeta)$ are involved in Eq. (7). Also, ζ_n^f is the ζ -coordinate of the neutral surface at the end of the process. The general structure of the solution in the ζa -space is illustrated in Fig. 2. If $s(a)$ were known, Eq. (5) would determine $a_c(\zeta)$ and, therefore, $s_c(\zeta)$. Thus, $s(a)$ is the only unknown function in the analysis of kinematics and this function should be found from the analysis of stress and damage.

3. Stress analysis and damage evolution

The only non-trivial equilibrium equation in the plane polar coordinate system $r\theta$ in terms of the radial and circumferential stresses has the form

$$\frac{\partial \sigma_r}{\partial r} + \frac{\sigma_r - \sigma_\theta}{r} = 0. \quad (8)$$

It is obvious that $\sigma_r \equiv \sigma_{\zeta\zeta}$ and $\sigma_\theta \equiv \sigma_{\eta\eta}$. The plane-strain yield condition in the case under consideration is

$$\sigma_r - \sigma_\theta = \pm \frac{2}{\sqrt{3}} \sigma_0 \Phi(\epsilon_{eq})(1 - D), \quad (9)$$

where the upper sign corresponds to the region $-1 \leq \zeta \leq \zeta_n$ and the lower sign to the region $\zeta_n \leq \zeta \leq 0$. Also, the function $\Phi(\epsilon_{eq})$ satisfies

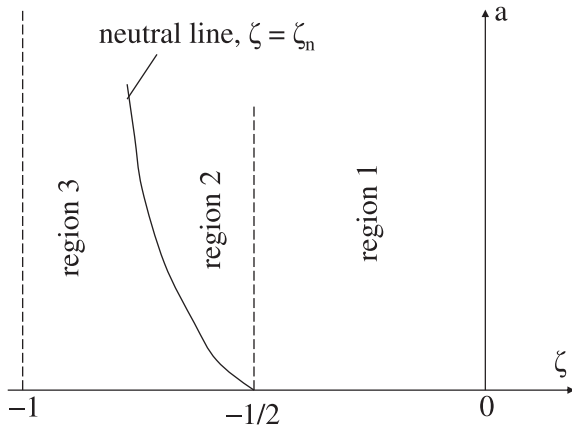


Fig. 2. General structure of the solution.

the condition $\Phi(0) = 1$, σ_0 is the initial yield stress in tension, and D is the damage parameter. Using Eq. (3) it is possible to replace r and differentiation with respect to r with ζ and differentiation with respect to ζ in Eq. (8). Then, with using Eq. (9),

$$\frac{\partial \sigma_r}{\partial \zeta} = \mp \frac{a \sigma_0 \Phi(\varepsilon_{eq})(1-D)}{\sqrt{3}(\zeta a + s)}. \quad (10)$$

The function $\Phi(\varepsilon_{eq})$ should be prescribed and ε_{eq} can be excluded by means of Eq. (7). The boundary conditions on the radial stress are

$$\sigma_r = 0 \quad (11)$$

for $\zeta = -1$ and $\zeta = 0$. Since there are the two boundary conditions for the differential equation of first order, the function $s(a)$ and, consequently, the neutral line position (see Eq. (5)) should be found from the solution to Eq. (10) simultaneously with constant of integration. Also, the radial stress must be continuous across the boundary of the aforementioned regions (Fig. 2). For material models with no damage parameter Eq. (10) is the only equation to be integrated numerically. In the case under consideration, Eq. (10) should be supplemented with a damage evolution law. A wide class of phenomenological damage evolution laws can be written in the form

$$\dot{D} = A \left(\frac{\sigma}{\sigma_{eq}}, \varepsilon_{eq}, D \right) \dot{\varepsilon}_{eq}, \quad (12)$$

where the overdot denotes the material derivative. In the case of plane strain deformation, the flow rule associated with the yield condition (9) gives $\sigma_z = \sigma = (\sigma_r + \sigma_\theta)/2$. Since the shear stresses in the cylindrical coordinate system vanish, the equivalent stress involved in (12) is given by $\sigma_{eq} = (\sqrt{3}/2)|\sigma_r - \sigma_\theta|$. In the Lagrangian coordinates, Eq. (12) can be rewritten, with the use of Eq. (6), as

$$\frac{\partial D}{\partial a} = \frac{1}{\sqrt{3}} A \left(\frac{\sigma}{\sigma_{eq}}, \varepsilon_{eq}, D \right) \frac{|\zeta + ds/da|}{(\zeta a + s)}. \quad (13)$$

The initial distribution of the damage parameter should be prescribed. A widely used assumption is

$$D = D_0 \quad (14)$$

for $a = 0$. Here D_0 is constant.

Once the solution for stress has been found, the bending moment per unit length is determined by integration (Alexandrov et al., 2006)

$$M = \frac{H^2}{2a} \int_{-1}^0 \sigma_{\theta\theta} d\zeta. \quad (15)$$

At the initial instant when $D = D_0$ and $\varepsilon_{eq} = 0$, the solution reduces to that for the rigid perfectly plastic material model. The latter is given in Hill (1950). It can be immediately found from this solution that $\zeta_n = -1/2$ at $a = 0$. Then, it follows from Eq. (5) that

$$ds/da = 1/2 \quad (16)$$

at $a = 0$. Moreover, at the initial instant

$$\sigma_r = 0 \text{ everywhere}$$

$$\sigma_\theta = \frac{2}{\sqrt{3}} \sigma_0 (1 - D_0) \text{ in the range } -1 \leq \zeta < -1/2 \quad (17)$$

$$\sigma_\theta = -\frac{2}{\sqrt{3}} \sigma_0 (1 - D_0) \text{ in the range } -1/2 < \zeta \leq 0.$$

The bending moment per unit length is determined from this equation as

$$M_0 = \frac{\sigma_0 (1 - D_0) H^2}{2\sqrt{3}}. \quad (18)$$

In the case of the rigid perfectly plastic material model the bending moment is constant throughout the process of deformation (Hill, 1950).

In order to facilitate numerical solution of Eqs. (10) and (13), the second derivative d^2s/da^2 at the initial instant can be found analytically. In particular, the solution of Eq. (10) in region 3 (Fig. 2) satisfying the boundary condition (11) at $\zeta = -1$ can be written in the form

$$\sigma_r = -\frac{a \sigma_0}{\sqrt{3}} \int_{-1}^{\zeta} \frac{\Phi(\varepsilon_{eq})(1-D)}{(za + s)} dz, \quad (19)$$

where z is an auxiliary variable of integration. Then, the radial stress acting at $\zeta = \zeta_n$ is

$$\sigma_{32} = -\frac{a \sigma_0}{\sqrt{3}} \int_{-1}^{\zeta_n} \frac{\Phi(\varepsilon_{eq})(1-D)}{(za + s)} dz. \quad (20)$$

The solution of Eq. (10) in region 2 (Fig. 2) satisfying the boundary condition $\sigma_r = \sigma_{32}$ at $\zeta = \zeta_n$ can be written in the form

$$\sigma_r = \sigma_{32} + \frac{a \sigma_0}{\sqrt{3}} \int_{\zeta_n}^{\zeta} \frac{\Phi(\varepsilon_{eq})(1-D)}{(za + s)} dz. \quad (21)$$

Then, the radial stress acting at $\zeta = -1/2$ is

$$\sigma_{21} = \sigma_{32} + \frac{a \sigma_0}{\sqrt{3}} \int_{\zeta_n}^{-1/2} \frac{\Phi(\varepsilon_{eq})(1-D)}{(za + s)} dz. \quad (22)$$

Finally, the solution of Eq. (10) in region 1 (Fig. 2) satisfying the boundary condition $\sigma_r = \sigma_{21}$ at $\zeta = -1/2$ can be written in the form

$$\sigma_r = \sigma_{21} + \frac{a \sigma_0}{\sqrt{3}} \int_{-1/2}^{\zeta} \frac{\Phi(\varepsilon_{eq})(1-D)}{(za + s)} dz. \quad (23)$$

Substituting the boundary condition (11) at $\zeta = 0$ into Eq. (23) gives

$$\sigma_{21} + \frac{a \sigma_0}{\sqrt{3}} \int_{-1/2}^0 \frac{\Phi(\varepsilon_{eq})(1-D)}{(za + s)} dz = 0. \quad (24)$$

Using Eqs. (5), (20) and (22) Eq. (24) can be transformed to

$$I_1 + I_2 - I_3 = 0, \quad (25)$$

where

$$I_1 = \int_{-ds/da}^{-1/2} \frac{\Phi(\varepsilon_{eq})(1-D)}{(za + s)} dz, \quad I_2 = \int_{-1/2}^0 \frac{\Phi(\varepsilon_{eq})(1-D)}{(za + s)} dz, \quad (26)$$

$$I_3 = \int_{-1}^{-ds/da} \frac{\Phi(\varepsilon_{eq})(1-D)}{(za + s)} dz.$$

Differentiating each of these integrals with respect to a and, then, putting $a = 0$ and taking into account Eqs. (2), (14) and (16) as well as the conditions $\varepsilon_{eq} = 0$ at the initial instant and $\Phi(0) = 1$ gives

$$\begin{aligned}
\left. \frac{\partial I_1}{\partial a} \right|_{a=0} &= 4(1-D_0) \left. \frac{d^2 s}{da^2} \right|_{a=0} + 16 \int_{-1/2}^{-1/2} \left\{ \left[(1-D_0) \frac{d\Phi}{d\epsilon_{eq}} \frac{\partial \epsilon_{eq}}{\partial a} \right]_{a=0} \right. \\
&\quad \left. - \frac{\partial D}{\partial a} \right|_{a=0} \left[\frac{1}{4} - \left(z + \frac{1}{2} \right) (1-D_0) \right] dz = 4(1-D_0) \left. \frac{d^2 s}{da^2} \right|_{a=0} \\
\left. \frac{\partial I_2}{\partial a} \right|_{a=0} &= 16 \int_{-1/2}^0 \left\{ \left[(1-D_0) \frac{d\Phi}{d\epsilon_{eq}} \frac{\partial \epsilon_{eq}}{\partial a} \right]_{a=0} - \frac{\partial D}{\partial a} \right|_{a=0} \left[\frac{1}{4} \right. \right. \\
&\quad \left. \left. - \left(z + \frac{1}{2} \right) (1-D_0) \right] dz = 4(1-D_0) \right. \\
&\quad \left. \frac{d\Phi}{d\epsilon_{eq}} \int_{-1/2}^0 \frac{\partial \epsilon_{eq}}{\partial a} \right|_{a=0} dz - 4 \int_{-1/2}^0 \frac{\partial D}{\partial a} \right|_{a=0} dz - 2(1-D_0), \\
\left. \frac{\partial I_3}{\partial a} \right|_{a=0} &= -4(1-D_0) \left. \frac{d^2 s}{da^2} \right|_{a=0} + 16 \int_{-1}^{-1/2} \left\{ \left[(1-D_0) \frac{d\Phi}{d\epsilon_{eq}} \frac{\partial \epsilon_{eq}}{\partial a} \right]_{a=0} \right. \\
&\quad \left. - \frac{\partial D}{\partial a} \right|_{a=0} \left[\frac{1}{4} - \left(z + \frac{1}{2} \right) (1-D_0) \right] dz = -4(1-D_0) \left. \frac{d^2 s}{da^2} \right|_{a=0} \\
&\quad + 4(1-D_0) \frac{d\Phi}{d\epsilon_{eq}} \int_{-1}^{-1/2} \frac{\partial \epsilon_{eq}}{\partial a} \right|_{a=0} dz - 4 \int_{-1}^{-1/2} \frac{\partial D}{\partial a} \right|_{a=0} dz + 2(1-D_0).
\end{aligned} \quad (27)$$

Here the derivative $d\Phi/d\epsilon_{eq}$ has been taken out the integral sign because it is solely a function ϵ_{eq} and $\epsilon_{eq} = 0$ at the initial instant. Since, by definition, $\partial \epsilon_{eq} / \partial t = \dot{\epsilon}_{eq}$ in the Lagrangian coordinates, the derivative $\partial \epsilon_{eq} / \partial a$ at the initial instant is determined with the use of Eqs. (2), (6), and (16) as

$$\left. \frac{\partial \epsilon_{eq}}{\partial a} \right|_{a=0} = \frac{4}{\sqrt{3}} \left[\zeta + \frac{1}{2} \right]. \quad (28)$$

Substituting Eq. (28) into Eq. (27) and, then, Eq. (27) into Eq. (25) differentiated with respect to a leads to

$$2(1-D_0) \left. \frac{d^2 s}{da^2} \right|_{a=0} - \int_{-1/2}^0 \frac{\partial D}{\partial a} \right|_{a=0} dz + \int_{-1}^{-1/2} \frac{\partial D}{\partial a} \right|_{a=0} dz - (1-D_0) = 0. \quad (29)$$

In the case of many damage evolution laws the function $A(\sigma/\sigma_{eq}, \epsilon_{eq}, D)$ involved in Eq. (12) vanishes for $\epsilon_{eq} = 0$. For such laws Eq. (29) simplifies to

$$\left. \frac{d^2 s}{da^2} \right|_{a=0} \equiv s_2^{(0)} = \frac{1}{2}. \quad (30)$$

4. Numerical solution

The approach developed is illustrated by numerical solution for the damage evolution law proposed in Hartley et al. (1997) assuming that $D_0 = 0$ in Eq. (14). In this case

$$A\left(\frac{\sigma}{\sigma_{eq}}, \epsilon_{eq}, D\right) = \alpha \exp\left(\frac{3}{2} \frac{\sigma}{\sigma_{eq}}\right) \epsilon_{eq}^{2/n}, \quad (31)$$

where α and n are material constants and, therefore, Eq. (30) is valid. The value of n is usually related to the hardening exponent. It is assumed in all calculations that $n = 0.25$ and the effect of α -value on the solution is studied. The function $\Phi(\epsilon_{eq})$ involved in Eq. (9) is taken in the form of Swift's law

$$\Phi(\epsilon_{eq}) = \left(1 + \frac{\epsilon_{eq}}{0.222}\right)^{0.25}. \quad (32)$$

The fracture criterion is

$$D = D_c, \quad (33)$$

where D_c is a material constant. It is assumed in all calculations that $D_c = 0.3$.

Suppose that the through thickness distribution of stress and damage parameter is known at $a = a_j$, i.e., those can be represented, in particular, as discrete functions of ζ . Also, the values of $s = s^{(j)}$, $ds/da = s_1^{(j)}$, and $d^2s/da^2 = s_2^{(j)}$ are supposed to be known at $a = a_j$. The function $s(a)$ in the interval $a_j \leq a \leq a_j + \Delta a = a_{j+1}$ can be approximated as

$$s(a) = s^{(j)} + s_1^{(j)}(a - a_j) + \frac{1}{4}(s_2^{(j)} + s_2^{(j+1)})(a - a_j)^2, \quad (34)$$

where $s_2^{(j+1)}$, the second derivative d^2s/da^2 at $a = a_{j+1}$, is unknown. It follows from Eq. (34) that

$$\begin{aligned}
s^{(j+1)} &= s^{(j)} + s_1^{(j)} \Delta a + \frac{1}{4}(s_2^{(j)} + s_2^{(j+1)})(\Delta a)^2, \\
s_1^{(j+1)} &= s_1^{(j)} + \frac{1}{2}(s_2^{(j)} + s_2^{(j+1)})\Delta a.
\end{aligned} \quad (35)$$

Using Eqs. (7) and (31) as well as the solution at $a = a_j$ the right hand side of Eq. (13) can be found at $a = a_j$ as a discrete function of ζ . Then, the through-thickness discrete distribution of the damage parameter at $a = a_{j+1}$ is approximated by

$$D^{(j+1)} = D^{(j)} + \left(\frac{\partial D}{\partial a} \right) \Big|_{a=a^{(j)}} \Delta a. \quad (36)$$

Eqs. (19)–(26) are valid at any value of a . Using Eqs. (5), (7), (32), (35), and (36) the integrals involved in Eq. (26) can be calculated numerically at $a = a_{j+1}$ for any value of $s_2^{(j+1)}$. Then, Eq. (25) has to be solved to determine the value of $s_2^{(j+1)}$. In order to start the numerical procedure described, Eqs. (2), (14), (16), (17), and (30) should be adopted at $a = a^{(1)} = 0$. The solution can be transformed into the physical space by means of Eqs. (3) and (4). In particular, for illustration of the through-thickness distribution of functions it is convenient to introduce the dimensionless coordinate in the form

$$X = \frac{r - R_{CD}}{H} = \sqrt{\frac{\zeta}{a} + \frac{s}{a^2}} - \sqrt{\frac{s}{a^2} - \frac{1}{a}}. \quad (37)$$

It is obvious that $X = 0$ at the concave surface CD (Fig. 1). Calculation has shown that the variation of h is negligible. Therefore, $X \approx 1$ at the convex surface AB . A similar result has been obtained from analytic solutions for various strain hardening materials with no damage evolution (Bruhns et al., 2003; Alexandrov and Hwang, 2010). On the other hand, solutions for some material models predict a significant change in the thickness of the sheet at large strains (see, for example, Zhu, 2007).

The through-thickness variation of the damage parameter at $\alpha = 0.8$, $\alpha = 1$ and $\alpha = 1.2$ is depicted in Figs. 3–5, respectively. Curves 1, 2 and 3 in each figure correspond to $H/R_{CD} = 0.3$, $H/R_{CD} = 0.5$ and $H/R_{CD} = 0.7$, respectively. Curve 4 corresponds to the stage of the process at which the fracture initiation occurs at the convex surface of the specimen according to the criterion (33). In particular, the maximum value of H/R_{CD} is $H/R_{CD}^{\min} = 1.46$ for $\alpha = 0.8$, $H/R_{CD}^{\min} = 1.1$ for $\alpha = 1$ and $H/R_{CD}^{\min} = 0.88$ for $\alpha = 1.2$. The variation of H/R_{CD}^{\min} with α is shown in Fig. 6. The through-thickness distribution of the radial and circumferential stresses is depicted in Figs. 7–12. As before, curves 1, 2, 3 and 4 correspond to $H/R_{CD} = 0.3$, $H/R_{CD} = 0.5$, $H/R_{CD} = 0.7$ and $H/R_{CD} = H/R_{CD}^{\min}$, respectively. Also, $\alpha = 0.8$ in Figs. 7 and 10, $\alpha = 1$ in Figs. 8 and 11, and $\alpha = 1.2$ in Figs. 9 and 12. Having the distribution of the circumferential stress, the bending moment can be calculated by means of Eq. (15). The variation of the dimensionless bending moment defined by $m = M/M_0$ where M_0 is given by Eq. (18) with H/R_{CD} is shown for several values of α in Fig. 13. In this figure, curves 1, 2, 3, 4, and 5 correspond to $\alpha = 1.2$, $\alpha = 1.1$, $\alpha = 1$, $\alpha = 0.9$, and $\alpha = 0.8$, respectively. Finally, the variation of the position of the neutral line, $X = X_n$, with H/R_{CD} is depicted in Fig. 14. The dependence of the value of X_n on α in the range of H/R_{CD} -values in which no fracture occurs is negligible.

The curve in Fig. 14 is for $\alpha = 0.8$ since the value of H/R_{CD}^{\min} is largest for this value of α in the interval considered, $0.8 \leq \alpha \leq 1.2$.

5. Conclusions

The general solution proposed describes the process of pure bending of rigid plastic material obeying an arbitrary law of isotropic hardening and an arbitrary law of damage evolution, assuming that the material is incompressible. An advantage of the method used is that numerical treatment has been reduced to solving two partial differential equations written in characteristic coordinates (Eqs. (10) and (13)).

The illustrative example has been presented for the hardening law in the form of Eq. (32) and the damage evolution law in the form of Eq. (31). Numerical results coincide with physical expectations. In particular, the magnitude of the damage parameter is rather low in the vicinity of the neutral line (Figs. 3–5). This is a consequence of the fact that the equivalent strain rate vanishes at the neutral line and the magnitude of the equivalent strain is low in the center of the specimen. Also, the magnitude of the damage parameter on the concave side of the specimen is less than on its convex side. This is a consequence of the fact that compressive hydrostatic stress delays fracture. The through-thickness distribution of the principal stresses is in general similar to that in hardening materials with no damage parameter. However, the through-thickness variation of the circumferential stress is not significant on each side of the neutral line. This can be explained by the competition between strain hardening and softening due to damage. This conclusion is confirmed by the variation of the bending moment with H/R_{CD} (Fig. 13). At the initial stage of the process, the bending moment increases with H/R_{CD} , as in the case of strain hardening materials. An effect of damage is revealed at a later stage when the magnitude of the bending moment attains a maximum and, then, decreases. Therefore, the difference from the rigid perfectly plastic bending moment is not significant on average.

An effect of α -value on solution behaviour follows physical expectations as well. In particular, the larger α -value, the more pronounced effect of the damage parameter is. A representative example is the variation of the bending moment (Fig. 13). In this case, the increase in α -value leads to the decrease in the maximum value of the bending moment.

It is of interest to compare the stress distributions found with the corresponding solution with no damage evolution. Formally, the solution with no damage evolution can be obtained from the present solution assuming that $\alpha = 0$ in Eq. (31). However, the analytic derivation can be advanced in the case of $D = 0$. In particular, replacing in Eq. (10) the derivative with respect to ζ with the derivative with respect to ε_{eq} by means of Eq. (7) gives

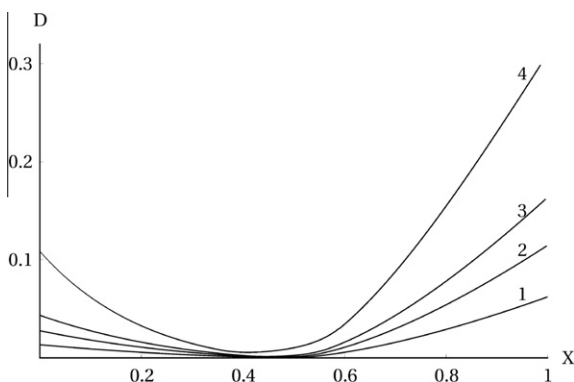


Fig. 3. Through-thickness distribution of the damage parameter at $\alpha = 0.8$ and several values of H/R_{CD} .

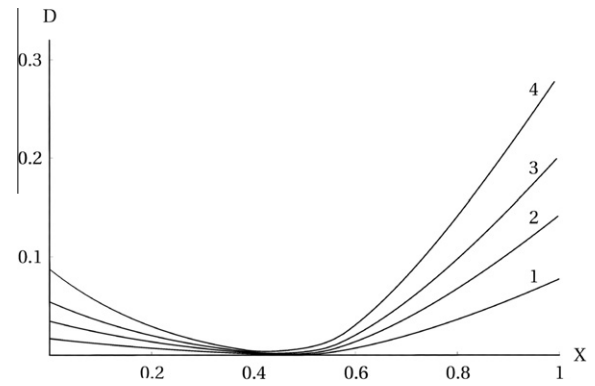


Fig. 4. Through-thickness distribution of the damage parameter at $\alpha = 1$ and several values of H/R_{CD} .

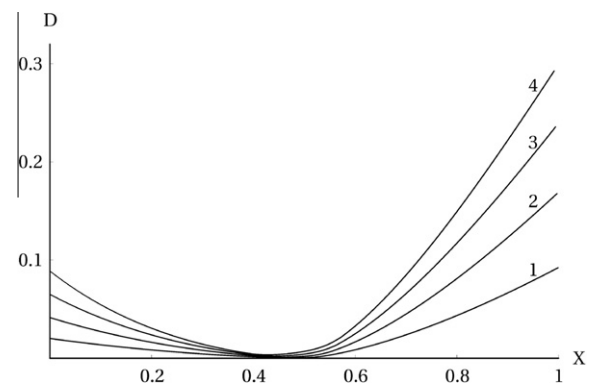


Fig. 5. Through-thickness distribution of the damage parameter at $\alpha = 1.2$ and several values of H/R_{CD} .

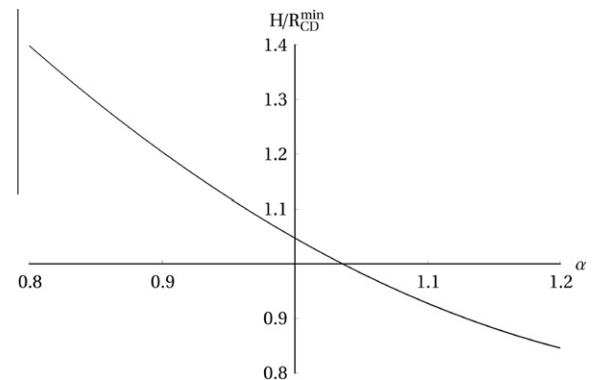


Fig. 6. Variation of the value of H/R_{CD} at which fracture at the convex surface occurs with α .

$$\frac{\partial \sigma_r}{\partial \varepsilon_{eq}} = \sigma_0 \Phi(\varepsilon_{eq}) \quad (38)$$

in regions 1 and 3 (Fig. 2). Substituting Eq. (32) into Eq. (38) and integrating with the use of the condition (17) result in

$$\begin{aligned} \frac{\sigma_r}{\sigma_0} &= \frac{0.222}{1.25} \left(1 + \frac{\varepsilon_{eq}}{0.222}\right)^{1.25} - \frac{0.222}{1.25} f_1(a), \\ \frac{\sigma_r}{\sigma_0} &= \frac{0.222}{1.25} \left(1 + \frac{\varepsilon_{eq}}{0.222}\right)^{1.25} - \frac{0.222}{1.25} f_3(a) \end{aligned} \quad (39)$$

in regions 1 and 3, respectively. Here $f_1(a)$ and $f_3(a)$ are arbitrary functions of a and $f_1(0) = f_3(0) = 1$. The equivalent strain in Eq. (39) should be excluded by means of Eq. (7). Eq. (39) are not particularly useful for solving Eq. (10) in the entire range of ζ , $-1 \leq \zeta \leq 0$, but for verifying the numerical code developed. For, once the

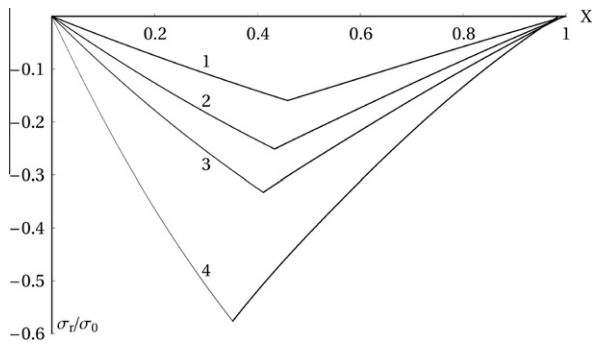


Fig. 7. Through-thickness distribution of the radial stress at $\alpha = 0.8$ and several values of H/R_{CD} .

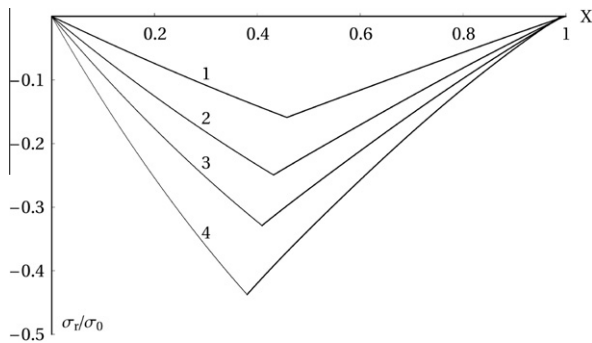


Fig. 8. Through-thickness distribution of the radial stress at $\alpha = 1$ and several values of H/R_{CD} .

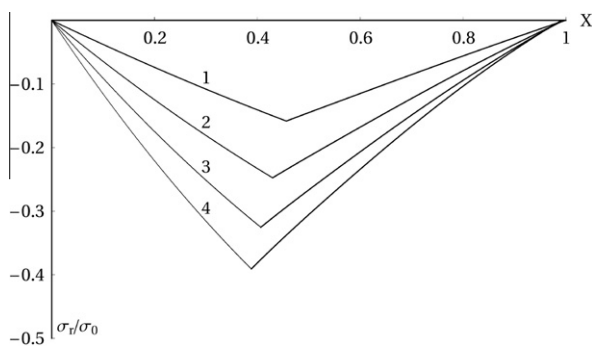


Fig. 9. Through-thickness distribution of the radial stress at $\alpha = 1.2$ and several values of H/R_{CD} .

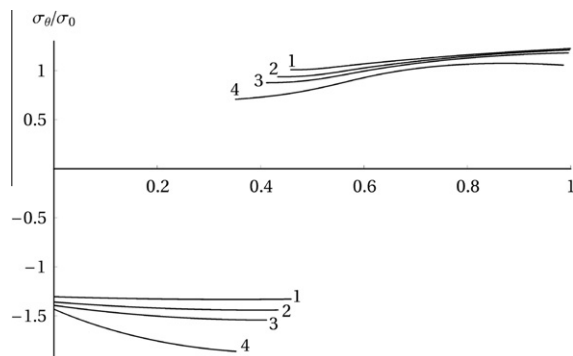


Fig. 10. Through-thickness distribution of the circumferential stress at $\alpha = 0.8$ and several values of H/R_{CD} .

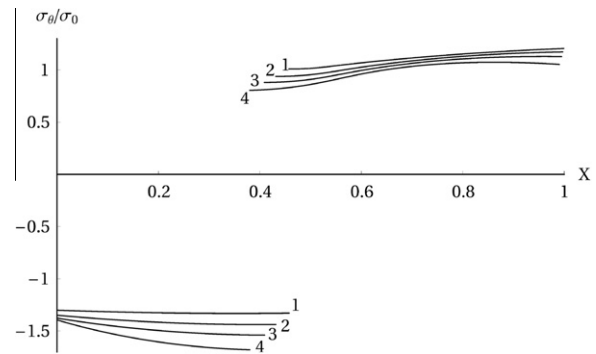


Fig. 11. Through-thickness distribution of the circumferential stress at $\alpha = 1$ and several values of H/R_{CD} .

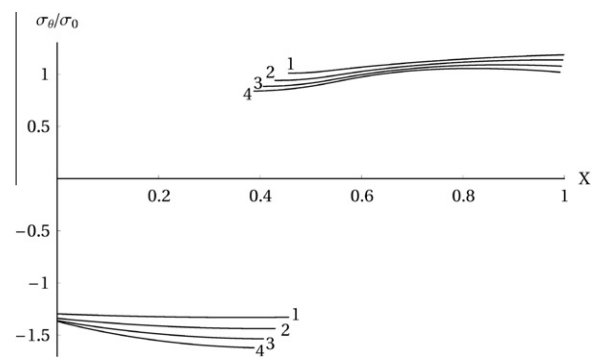


Fig. 12. Through-thickness distribution of the circumferential stress at $\alpha = 1.2$ and several values of H/R_{CD} .

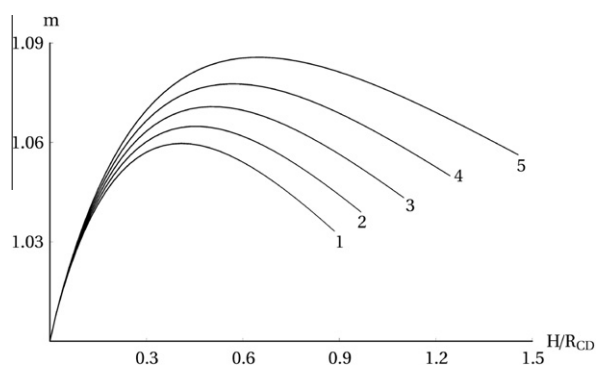


Fig. 13. Variation of the dimensionless bending moment with H/R_{CD} at several α -values.

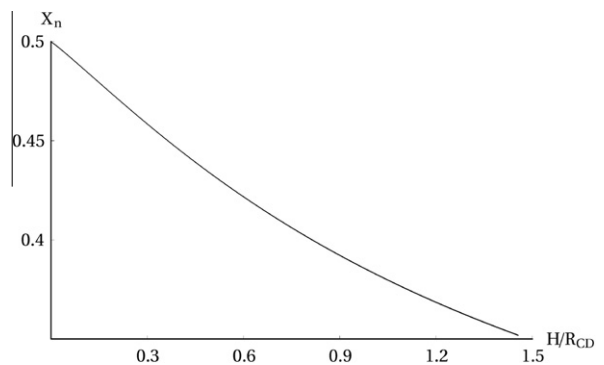


Fig. 14. Position of the neutral line with H/R_{CD} for $\alpha = 0.8$.

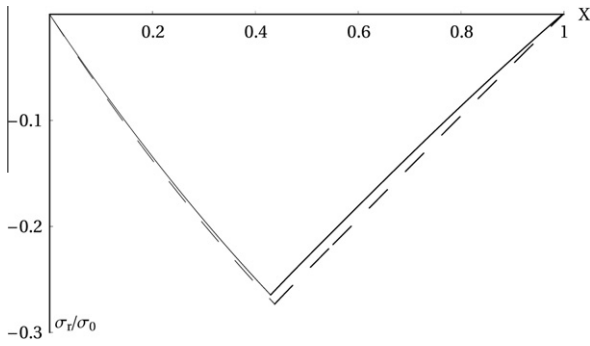


Fig. 15. Distribution of the radial stress at $H/R_{CD} = 0.5$.

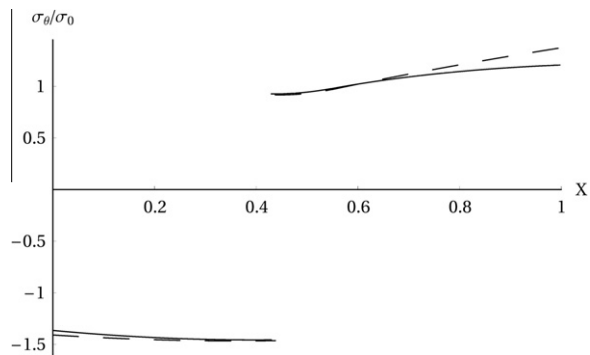


Fig. 16. Distribution of the circumferential stress at $H/R_{CD} = 0.5$.

numerical solution has been found, the values of the equivalent strain at $\zeta = 0$ and $\zeta = -1$ are known, say $\varepsilon_1(a)$ and $\varepsilon_3(a)$. Then, substituting Eq. (7) into Eq. (39) and taking into account that $\sigma_r = 0$ at $\zeta = 0$ and $\zeta = -1$ give

$$f_1(a) = \left(1 + \frac{\varepsilon_1(a)}{0.222}\right)^{1.25}, \quad f_3(a) = \left(1 + \frac{\varepsilon_3(a)}{0.222}\right)^{1.25}.$$

The radial stress distributions in regions 1 and 3 obtained after substituting these functions and (7) into Eq. (39) can be compared to the numerical solution.

The distributions of the radial and circumferential stresses at $H/R_{CD} = 0.5$ are depicted in Figs. 15 and 16, respectively. The dashed lines correspond to $\alpha = 0$ (no damage), and solid lines to $\alpha = 1.2$.

Acknowledgment

The main part of this work was done while the first author was with the University of Franche-Comte (Besancon, France) as a vis-

iting professor. S.A. also acknowledges support from Grant RFBR-10-08-00083.

References

- Alexandrov, S., Hwang, Y.-M., 2009. The bending moment and springback in pure bending of anisotropic sheets. *Int. J. Solids Struct.* 46, 4361–4368.
- Alexandrov, S., Hwang, Y.-M., 2010. Plane strain bending with isotropic strain hardening at large strains. *Trans. ASME J. Appl. Mech.* 77, 064502.
- Alexandrov, S., Kim, J.-H., Chung, K., Kang, T.-J., 2006. An alternative approach to analysis of plane-strain pure bending at large strains. *J. Strain Anal. Eng. Des.* 41, 397–410.
- Andrade Pires, F.M., Cesar de Sa, J.M.A., Costa Sousa, L., Natal Jorge, R.M., 2003. Numerical modelling of ductile plastic damage in bulk metal forming. *Int. J. Mech. Sci.* 45, 273–294.
- Atkins, A., 1996. Fracture in forming. *J. Mater. Process. Technol.* 56, 609–618.
- Behrens, A., Just, H., 2002. Verification of the damage model of effective stresses in cold and warm forging operations by experimental testing and FE simulations. *J. Mater. Process. Technol.*, 295–301.
- Boers, S.H.A., Geers, M.G.D., Kouznetsova, V.G., 2010. Contactless and frictionless pure bending. *Exp. Mech.* 50, 683–693.
- Bonora, N., 1997. A nonlinear CDM model for ductile failure. *Eng. Fract. Mech.* 58, 11–28.
- Bruhns, O.T., Gupta, N.K., Meyers, A.T.M., Xiao, H., 2003. Bending of an elastoplastic strip with isotropic and kinematic hardening. *Arch. Appl. Mech.* 72, 759–778.
- Chandranth, S., Pandey, P.C., 1993. A new ductile damage evolution model. *Int. J. Fract.* 60, R73–R76.
- Dadras, P., Majless, S.A., 1982. Plastic bending of work hardening materials. *Trans. ASME J. Eng. Ind.* 104, 224–230.
- Gao, X.-L., 1994. Finite deformation elasto-plastic solution for the pure bending problem of a wide plate of elastic linear-hardening material. *Int. J. Solids Struct.* 31, 1357–1376.
- Gurson, A.L., 1977. Continuum theory of ductile rupture by void nucleation and growth: Part 1 – Yield criteria and flow rules for porous ductile media. *Trans. ASME J. Eng. Mater. Technol.* 99, 2–15.
- Hambli, R., 2001. Comparison between Lemaitre and Gurson damage models in crack growth simulation during blanking process. *Int. J. Mech. Sci.* 43, 2769–2790.
- Hartley, P., Hall, F.R., Chiou, J.M., Pillinger, I., 1997. Elastic-plastic finite-element modelling of metal forming with damage evolution. In: Predeleanu, M., Gilormini, P. (Eds.), *Advanced Methods in Materials Processing Defects*. Elsevier, Amsterdam, pp. 135–142.
- Hill, R., 1950. *The Mathematical Theory of Plasticity*. Clarendon Press, Oxford.
- Lemaitre, J., 1985. A continuous damage mechanics model for ductile fracture. *Trans. ASME J. Eng. Mater. Technol.* 107, 83–89.
- Lyamina, E.A., 2006. Plastic bending of a strip for a yield criterion depending on the mean stress. *J. Appl. Mech. Tech. Phys.* 47, 249–253.
- Tai, W.H., 1990. Plastic damage and ductile fracture in mild steels. *Eng. Fract. Mech.* 37, 853–880.
- Tan, Z., Persson, B., Magnusson, C., 1995. Plastic bending of anisotropic sheet metals. *Int. J. Mech. Sci.* 37, 405–421.
- Tvergaard, V., Needleman, A., 1984. Analysis of the cup-cone fracture in a round tensile bar. *Acta Metall.* 32, 157–169.
- Verguts, H., Sowerby, R., 1975. The pure plastic bending of laminated sheet metals. *Int. J. Mech. Sci.* 17, 31–51.
- Wang, C., Kinzel, G., Altan, T., 1993. Mathematical modeling of plane-strain bending of sheet and plate. *J. Mater. Process. Technol.* 39, 279–304.
- Zhu, H.X., 2007. Large deformation pure bending of an elastic plastic power-law-hardening wide plate: analysis and application. *Int. J. Mech. Sci.* 49, 500–514.